Ocean Engineering 243 (2022) 110260

Contents lists available at ScienceDirect

Ocean Engineering

journal homepage: www.elsevier.com/locate/oceaneng

Control oriented modeling of a twin thruster autonomous surface vehicle☆

Enrico Simetti *, Giovanni Indiveri

DIBRIS, University of Genova (ISME node), Via all'Opera Pia 13, Genova, Italy

ARTICLE INFO

Keywords:
Marine robotics
Autonomous surface vehicles
Modeling
Identification

ABSTRACT

This work investigates and identifies a first principles maneuvering model for a small size robotic twin thruster autonomous surface vessel (ASV) that includes and explains the sources of nonlinearity and asymmetry of this class of robots. With respect to state of the art ASV models, the proposed one accounts for the effects generating a transverse thrust, explaining the asymmetric turning radii. The model also accounts for the need to adapt the hydrodynamic derivatives when the ASV performs large or tight turns. An experimental dataset has been acquired using the ULISSE ASV and it is used to support the proposed model in comparison to the "baseline" one often used in the literature. The improved precision of the proposed model in fitting experimental data is a necessary prerequisite to design model-based motion controller and navigation systems with enhanced performance.

1. Introduction

The recent developments of autonomous marine vehicles have enabled new interesting applications where they can reduce the use of large manned ships with high operational costs. Such applications include, just to cite a few, search and rescue, hydrological and environmental monitoring, maritime security, geotechnical surveying, and offshore installation protection (Zereik et al., 2018; Elkins et al., 2010; Simetti et al., 2021; Peng et al., 2020).

ASVs started to be a topic of interest for research and civil applications since early 1990s. Massachusetts Institute of Technology (MIT) developed ARTEMIS in 1993 (Vaneck et al., 1996), an ASV designed for various missions, including the collection of bathymetry data. A few new platforms, including ACES (Manley, 1997) and SCOUT (Curcio et al., 2005), were built to continue the work on hydrographic surveys and as testbed for robust control solutions. Several prototypes have been then developed since early 2000s, including MESSIN (Majohr and Buch, 2006), IST-ID's DELFIM (Alves et al., 2006), Charlie (Caccia et al., 2006), ROAZ (Ferreira et al., 2009), Springer (Naeem et al., 2008), Lake Wivenhoe ASV (Dunbabin et al., 2009) and SSC-SD (Ebken et al., 2005). A relatively recent review of ASV systems, and their current design challenges is reported in Liu et al. (2016).

In general, an ASV model can be established based on physical principles with some necessary model reductions. However, the establishment of an accurate ASV model is difficult, expensive, and time-consuming (Peng et al., 2020), as it is affected by several nonlinearities. In Eriksen and Breivik (2017) a control oriented modeling and identification procedure is proposed, with a particular focus on a single-rigid hull inflatable ASV that operates in the whole range of speed regions that a surface vehicle can cover, namely the displacement, semi-displacement and planing regions. The proposed modeling and identification technique does not include the thruster's model explicitly. In Sonnenburg and Woolsey (2013) the planar motion modeling for a single-hull ASV is developed, including a comparative evaluation of several experimentally identified models over a wide range of speeds and planing conditions, focusing their analysis on a modified rigid hull inflatable boat with automated throttle and steering.

Concerning twin-hull ASVs, a particle swarm based modeling approach is proposed in Wirtensohn et al. (2013) to model the ASV CaRoLIME. The model was obtained sequentially, as a suitable subsets of parameters have been identified utilizing dedicated maneuvers. In particular, the identification of surge dynamics was first accomplished by executing an almost straight line motion; then propeller thruster parameters were identified with the catamaran first tied to a poller while measuring the thrust force, then further straight line motion experiments were performed with different propeller rates. Finally, the steering dynamics parameter were estimated using two motion patterns, namely a zigzag- and a spiral-maneuver. A trajectory tracking nonlinear model predictive control solution for a twin-hull ASV is instead addressed in Guerreiro et al. (2014). The actuation model builds on standard ones available in the literature (Fossen, 2011) and it includes saturation nonlinearities but in the assumption that the motors can only generate positive thrust. However, experimental results

☆ This research did not receive any specific grant from funding agencies in the public, commercial, or not-for-profit sectors.
* Corresponding author.
E-mail address: enrico.simetti@unige.it (E. Simetti).
URL: http://www.isme.unige.it (E. Simetti).

https://doi.org/10.1016/j.oceaneng.2021.110260
Received 5 May 2021; Received in revised form 1 September 2021; Accepted 22 November 2021
Available online 9 December 2021

here discussed confirm that motors may also generate negative thrust, particularly so when moving on high curvature paths.

The ASV models typically used in the literature often neglect the fact that propellers also generate a transverse thrust. For single-screw vessels the influence of transverse thrust on maneuvering is entirely determined by the "paddle wheel effect" (see Carlton (2018), chapter 22), sometimes also called "propeller walk". The effect is called in such a way since the propeller moves the afterbody of the ship in the direction of rotation, i.e., in the sense of a paddle wheel moving relative to the sea bottom. The direction of this lateral force changes with the direction of propeller rotation, namely if the propeller is left or right-handed and with ahead or astern thrust. For twin-screws vessels, in addition to the aforementioned paddle wheel effect, lateral forces arise also for pressure differential on the hull, caused by reversing thrust of the propellers, and by shaft eccentricity (see Carlton (2018), chapter 22). These effects are further exacerbated if the two propellers are not counter rotating (i.e., if they are both right or left handed). These lateral forces generate an asymmetry in steering capabilities. To model this asymmetry, Ref. Peeters et al. (2018) suggests to use two set of parameters building an asymmetric virtual rudder Nomoto model. In Marquardt et al. (2013) the problem of propeller walk leads to very different turning radii, but it is not thoroughly modeled. The authors simply add a correction bias for obtaining straight motion in open-loop. A deep learning-based dynamic model identification method is proposed in Woo et al. (2018) and it is compared to a simplified maneuvering model, outperforming it. However, several effects were not considered in the maneuvering model, such as the wake effect on the thrusters and the asymmetric steering generated by the transverse thrust (Peeters et al., 2018) (the ASV employed in Peeters et al. (2018) is the same as the one in Woo et al. (2018)).

The control of vessels with uncertain dynamical models has received increasing interest in the recent years. In Skjetne et al. (2004), a maneuvering model for a model-ship is found, partially identified in a naval tank, and an adaptive controller is derived to deal with the unknown turning dynamics. The work (Du et al., 2018) considers the problem of dynamic position of a ship under unknown model parameters and unknown time-varying disturbance, proposing a robust adaptive control law which achieves the global asymptotic regulation of the positioning errors. The paper (Haseltalab and Negenborn, 2019) also considers uncertainty in propeller dynamics, and proposes an adaptive control based on a neural network to estimate the unmodeled dynamics.

In this work we aim to investigate and identify a first principles maneuvering model for a catamaran ASV which includes and explains the sources of nonlinearity and asymmetry of this class of vessels. The motivation of this work is that the improved precision of the proposed model in fitting experimental data is a necessary prerequisite to design model-based motion controller and navigation systems with enhanced performance. The original contributions of this manuscript can be summarized as follows:

- C_1 An integrated steady state ASV and thrusters model is presented. It models the asymmetry of the propeller thrust and its steady state wake effects in four quadrants. Furthermore, the effects generating a transverse thrust are also modeled, explaining the asymmetric turning radii. Finally, during tight turns, when the instantaneous center of rotation (ICR) lies between the hulls, the hydrodynamic derivatives of the lumped Fossen model (Fossen, 2011) cannot be assumed to be the same ones as when the vessel is proceeding straight or on large radius curves. Accounting for this model parameters change is key to explain the behavior of the vessel in tight turns and represents an entirely novel contribution of this work.
- C_2 The proposed steady state model can be effectively identified with field tests exploiting standard navigation and actuator data. Rather than separately identifying the vehicle hull's hydrodynamic derivatives and the thruster model, the proposed approach aims at concurrently identifying the model linking the steady state motion state variables to the actuation control inputs. This is indeed the most relevant kind of model for the design of the guidance, navigation and control sub-systems. An experimental data set has been acquired using the ULISSE ASV, showing how the proposed model and identification techniques allow capturing the asymmetric and nonlinear behavior of the ASV more accurately with respect to the approach normally used in the literature.

To the aim of showing the aforementioned contributions, the paper is structured as follows. Section 2 presents the "baseline" model, which represents the typical state of the art approach to ASV modeling. Section 3 presents the proposed model for a catamaran ASV, while its inverse model is discussed in Section 4. The successive Section 5 describes the proposed identification procedure. Section 6 first presents the ULISSE catamaran developed by ISME - University of Genova, which has been used to gather the experimental data, and then it discusses the validation of the proposed model on the data set itself. Finally, conclusions are reported in Section 7.

2. Baseline model

2.1. ASV model

For a marine craft restricted to operate in the horizontal plane (surge, sway and yaw), three generalized positions and velocities are needed to describe its motions (Fossen, 2011):

$$\boldsymbol{\eta} = \begin{bmatrix} x & y & \psi \end{bmatrix}^\top, \tag{1}$$

$$\boldsymbol{\nu} = \begin{bmatrix} u & v & r \end{bmatrix}^\top, \tag{2}$$

where x, y are the coordinates with respect to North and East and ψ is the heading of the vehicle with respect to the North and where u, v are the components of the inertial linear velocity vector projected in the body frame (u is surge and v is sway) and r is the yaw rate, i.e. the angular velocity about the vertical axis. The body frame has its z-axis pointing downwards and it is located at the center of the vehicle in between the two hulls where the navigation sensors are installed and in the proximity of the center of mass. Pitch, roll and heave motions and their possible couplings with the horizontal plane degrees of freedom are neglected.

Following Fossen (2011, 2012), the 3D maneuvering model is given by the following

$$\begin{aligned} \dot{\boldsymbol{\eta}} &= \boldsymbol{J}(\boldsymbol{\eta})\boldsymbol{\nu} \\ \boldsymbol{\nu}_r &\triangleq \boldsymbol{\nu} - \boldsymbol{\nu}_c \\ \boldsymbol{M}\dot{\boldsymbol{\nu}}_r + \boldsymbol{C}(\boldsymbol{\nu}_r)\boldsymbol{\nu}_r + \boldsymbol{D}(\boldsymbol{\nu}_r)\boldsymbol{\nu}_r &= \boldsymbol{\tau}_c(\boldsymbol{n}) \end{aligned} \tag{3}$$

where:

- $\boldsymbol{\nu}_c$ is an irrotational and constant (in the inertial frame) current velocity.
- $\boldsymbol{M} = \boldsymbol{M}_{RB} + \boldsymbol{M}_A > 0$ is the inertia matrix of the ASV including its added mass effects.
- $\boldsymbol{C}(\boldsymbol{\nu}_r) = \boldsymbol{C}_{RB}(\boldsymbol{\nu}_r) + \boldsymbol{C}_A(\boldsymbol{\nu}_r)$ is the sum rigid-body Coriolis and centripetal matrix $\boldsymbol{C}_{RB}(\boldsymbol{\nu}_r)$ and the hydrodynamic Coriolis and centripetal matrix $\boldsymbol{C}_A(\boldsymbol{\nu}_r)$. Matrix $\boldsymbol{C}(\boldsymbol{\nu}_r)$ can always be parametrized such that it is skew-symmetric, i.e. $\boldsymbol{C}(\boldsymbol{\nu}_r) = -\boldsymbol{C}(\boldsymbol{\nu}_r)^\top$.
- $\boldsymbol{D}(\boldsymbol{\nu}_r)$ represents the total hydrodynamic damping matrix, which is real and strictly positive $\boldsymbol{D}(\boldsymbol{\nu}_r) > \boldsymbol{0}$, $\forall\ \boldsymbol{\nu}_r$.
- $\boldsymbol{J}(\boldsymbol{\eta})$ is the Jacobian matrix linking the linear and angular body velocities (with components on the body frame) to the linear absolute velocities (with components on the inertial frame) and the Euler angles derivatives, which for the reduced 3D model is

$$\boldsymbol{J}(\boldsymbol{\eta}) = \begin{bmatrix} \cos(\psi) & -\sin(\psi) & 0 \\ \sin(\psi) & \cos(\psi) & 0 \\ 0 & 0 & 1 \end{bmatrix}. \tag{4}$$

Denoting with $\begin{bmatrix} x_G & y_G & z_G \end{bmatrix}^\top$ the position of the center of gravity in body frame, following (Fossen, 2011) the $\boldsymbol{C}_A$ and $\boldsymbol{C}_{RB}$ matrices result in:

$$\boldsymbol{C}_A(\boldsymbol{\nu}_r) = \begin{bmatrix} 0 & 0 & +Y_{\dot{v}}\, v_r + Y_{\dot{r}}\, r \\ 0 & 0 & -X_{\dot{u}}\, u_r \\ -Y_{\dot{v}}\, v_r - Y_{\dot{r}}\, r & X_{\dot{u}}\, u_r & 0 \end{bmatrix}, \tag{5}$$

$$\boldsymbol{C}_{RB}(\boldsymbol{\nu}_r) = \begin{bmatrix} 0 & 0 & -m(x_G\, r + v_r) \\ 0 & 0 & -m(y_G\, r - u_r) \\ m(x_G\, r + v_r) & m(y_G\, r - u_r) & 0 \end{bmatrix},$$

where m is the ASV mass and the standard notation (Society of Naval Architects and Marine Engineers, 1950) has been used for the hydrodynamic derivatives. In Eq. (3) the added mass matrix is assumed to be diagonal and in Eq. (5) the coupling terms eventually related to the hydrodynamic derivatives $X_{\dot{v}}$ and $X_{\dot{r}}$ are neglected as usually done for surface ships (Fossen, 2011).

The drag is typically assumed to include both a linear and quadratic term, i.e.

$$\begin{aligned} \boldsymbol{D}(\boldsymbol{\nu}_r) = &-\mathrm{diag}(X_u, Y_v, N_r) \\ &- \mathrm{diag}(X_{u|u|}\,|u_r|, Y_{v|v|}\,|v_r|, N_{r|r|}\,|r|). \end{aligned} \tag{6}$$

It should be noticed that the hydrodynamic terms are valid near an operating point (Fossen, 2011). However, the works available in the literature typically identify one value for each of these terms and use them independently from the current state of the robot. This means using the same parameters for tight turns or high speed cruising.

Finally, $\boldsymbol{n} \triangleq \begin{bmatrix} n_p & n_s \end{bmatrix}^\top$ is the collection of the RPM of the port and starboard motors and $\boldsymbol{\tau}_c(\boldsymbol{n})$, in the body frame, can be expressed as

$$\boldsymbol{\tau}_c(\boldsymbol{n}) \triangleq \boldsymbol{B}\boldsymbol{f}(\boldsymbol{n}) \triangleq \begin{bmatrix} 1 & 1 \\ 0 & 0 \\ d & -d \end{bmatrix} \begin{bmatrix} F_p(n_p) \\ F_s(n_s) \end{bmatrix} = \begin{bmatrix} F_p(n_p) + F_s(n_s) \\ 0 \\ d(F_p(n_p) - F_s(n_s)) \end{bmatrix}, \tag{7}$$

where $F_p(n_p)$ and $F_s(n_s)$ are the port and starboard longitudinal forces exerted by the thrusters on the body and d is the distance between each motor and the central point of the catamaran along the transversal axis. In the following, whenever a port/starboard independent relationship is considered, the p and s subscripts will be omitted, e.g., when the generic force $F(n)$ produced by a thruster is considered.

2.2. Thruster models

Several models exist for the propeller revolution rate to thrust relationship, see for example Pivano et al. (2009), Whitcomb and Yoerger (1999), Bachmayer et al. (2000) and Häusler et al. (2015). Due to the interactions with the hulls, these models can be very complicated and often simplified relationships are instead employed, especially for control purposes (Caccia et al., 2008). As our work focuses on identifying a steady state integrated ASV-thrusters model, here we will consider steady state thruster models, neglecting the acceleration of the fluid.

In such a context, one of the most frequently adopted propeller thrusters model is the bilinear model proposed by (Fossen, 1994):

$$F(u_m, n) = b_1 |n| n - b_2 |n| u_m, \quad b_1 > 0, b_2 \geq 0, \tag{8}$$

where the constant b_1 is the thrust coefficient, the constant b_2 includes the wake factor and where u_m is the linear velocity of the catamaran at the motor point, thus for port (p) and starboard (s) sides we have

$$\begin{aligned} u_{m,p} &= u_r + rd, \\ u_{m,s} &= u_r - rd. \end{aligned} \tag{9}$$

The factors b_1 and b_2 are expected to be different if $n > 0$ and $n < 0$. More sophisticated models also distinguish the terms depending on the sign of the water velocity u_m, yielding a four quadrant representation

$$\begin{bmatrix} b_1 & b_2 \end{bmatrix} = \begin{cases} \begin{bmatrix} b_1^{++} & b_2^{++} \end{bmatrix}, & \text{if } n \geq 0, u_m \geq 0 \\ \begin{bmatrix} b_1^{+-} & b_2^{+-} \end{bmatrix}, & \text{if } n \geq 0, u_m < 0 \\ \begin{bmatrix} b_1^{-+} & b_2^{-+} \end{bmatrix}, & \text{if } n < 0, u_m \geq 0 \\ \begin{bmatrix} b_1^{--} & b_2^{--} \end{bmatrix}, & \text{if } n < 0, u_m < 0 \end{cases}. \tag{10}$$

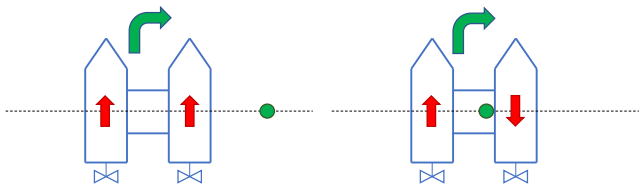

Fig. 1. (left) During cruising, the catamaran may follow curves characterized by an instantaneous center of rotation (green dot) lying outside of the hulls: in this case, both hulls will move forward (red arrows). In tight curves, the instantaneous center of rotation can lie between the hulls, causing one hull to move forward and the other in reverse, while the center of mass continues moving forward (right). (For interpretation of the references to color in this figure legend, the reader is referred to the web version of this article.)

3. Proposed model

3.1. Drag at different operating points

The first improvement of the proposed model with respect to the state of the art "baseline" approach is to model two different operating points regarding the angular drag. In particular, with reference to Fig. 1, let us consider two cases. In the first one (left hand side of the figure), the ASV is proceeding with a surge and yaw rate combination such that the instantaneous center of rotation (ICR) lies outside of the starboard hull. In this case, both hulls will move forward whilst rotating clockwise. In the second case (right hand side of the figure), the surge and yaw rate combination is different and the ICR lies in-between the two hulls, on the right side of the center of mass. In such a case, while both hulls will rotate clockwise, the port side hull will move forward, whilst the starboard side hull will move backward. Clearly, the second scenario is expected to have larger hydrodynamic derivatives, since one of the two hulls is moving backwards (and the hull is not optimized for such a movement, see Figs. 1 and 3).

To model these two different operating points, we propose to use the following drag equations

$$\begin{aligned} \boldsymbol{D}(\boldsymbol{\nu}_r) = &-\mathrm{diag}(X_u, Y_v, \alpha N_r + (1-\alpha) N_r^-) \\ &- \mathrm{diag}(X_{u|u|}\,|u_r|, Y_{v|v|}\,|v_r|, (\alpha N_{r|r|} + (1-\alpha) N_{r|r|}^-)\,|r|). \end{aligned} \tag{11}$$

where N_r and $N_{r|r|}$ are the coefficients for the angular drag hydrodynamic derivatives when both hulls move forward, and N_r^-, $N_{r|r|}^-$ are the ones when one of the two hulls is moving backwards. The transition from a set of coefficients to the other is done through the parameter α defined as follows

$$\alpha = \begin{cases} 1, & \text{if the ICR lies outside hulls} \\ 0, & \text{if the ICR lies in between hulls} \\ \gamma, & \text{otherwise} \end{cases}, \tag{12}$$

where $\gamma \in [0, 1]$ represents the fraction of the width of a single hull that is moving forward. The fraction γ can be computed from the position of the ICR, which in turn depends on the surge u_r and yaw rate r velocities, and the geometry of the ASV hulls, namely

$$\gamma = \left(\left| \frac{u_r}{r} \right| - d_h \right) / w_h, \tag{13}$$

where d_h is the transversal distance from the longitudinal axis to the beginning of the hull, and w_h is the width of the hull itself.

Owing to the same reason, the $\boldsymbol{C}_A(\boldsymbol{\nu}_r)$ matrix is modified as it follows

$$\boldsymbol{C}_A(\boldsymbol{\nu}_r) = \begin{bmatrix} 0 & 0 & Y_{\dot{v}}\, v_r + (\alpha Y_{\dot{r}} + (1-\alpha)Y_{\dot{r}}^-)\, r \\ 0 & 0 & -X_{\dot{u}}\, u_r \\ -Y_{\dot{v}}\, v_r - (\alpha Y_{\dot{r}} + (1-\alpha)Y_{\dot{r}}^-)\, r & X_{\dot{u}}\, u_r & 0 \end{bmatrix}. \tag{14}$$

Of course, the same reasoning could be applied for the surge drag. However, due to the dimensions and the shape of the hulls of the ULISSE ASV, full backward motions are never performed due high amounts of water raised by the thrusters toward the deck. Hence, modeling different surge operating points is not developed further in this work.

3.2. Modeling transverse thrust

In the baseline model, the only forces acting on the vessel are generated by the two thrusters in the longitudinal direction (see (7)). However, it is known that the propeller will move the afterbody of the ship in the direction of its rotation: that is in the sense of a paddle wheel relative to the sea bottom (see Carlton (2018), chapter 22). The paddle wheel effect is especially predominant in vessels with a single propeller, or with non-counterotating twin screws (Peeters et al., 2018; Marquardt et al., 2013), as it the case at hand. The pressure differential on the hulls caused by reversing thrusts of the propellers, and shaft eccentricity also produce a lateral force and turning moment (see Carlton (2018), chapter 22).

To model these effects, we propose to represent the total forces acting on the body of the ASV as it follows:

$$\begin{aligned} \boldsymbol{\tau}_c(\boldsymbol{n}) = \boldsymbol{B}\boldsymbol{f}(\boldsymbol{n}) &= \begin{bmatrix} 1 & 1 \\ k_p & k_s \\ d + l k_p & -d + l k_s \end{bmatrix} \begin{bmatrix} F_p(n_p) \\ F_s(n_s) \end{bmatrix} \\ &= \begin{bmatrix} F_p(n_p) + F_s(n_s) \\ k_p F_p(n_p) + k_s F_s(n_s) \\ d(F_p(n_p) - F_s(n_s)) + l(k_p F_p(n_p) + k_s F_s(n_s)) \end{bmatrix} \end{aligned} \tag{15}$$

where now a lateral force $k_p F_p(n_p) + k_s F_s(n_s)$ is introduced, together with its corresponding moment through the longitudinal distance l between the motors and the center of mass. The parameter k_p is defined as

$$k_p = \begin{cases} k^+ > 0, & \text{if } n_p \geq 0 \\ k^- > 0, & \text{if } n_p < 0, \end{cases} \tag{16}$$

since in general these effects are not symmetric with respect to the propeller speed, due to the interactions between the wake, the propeller and the hull. In fact, it is expected that a larger lateral force is exerted when the propeller spins in reverse. A similar relationship holds for k_s. As a final remark, note that now the matrix $\boldsymbol{B}$ in Eq. (15) actually results as a function of $\boldsymbol{n}$, since its coefficients k_p and k_s depend on the sign of their respective thruster speed.

3.3. Model at steady state

In this work, we focus on the identification of the hydrodynamic derivatives, thruster motor parameters and transverse thrust coefficients. These parameters can be identified at steady state. Hence, it is convenient to analyze the resulting steady state model, which can be expressed as

$$\boldsymbol{C}(\boldsymbol{\nu}_r)\boldsymbol{\nu}_r + \boldsymbol{D}(\boldsymbol{\nu}_r)\boldsymbol{\nu}_r \triangleq \boldsymbol{\tau}^*(\boldsymbol{\nu}_r) = \boldsymbol{\tau}_c(\boldsymbol{n}). \tag{17}$$

Denoting the components of $\boldsymbol{\tau}^*(\boldsymbol{\nu}_r)$ as:

$$\boldsymbol{\tau}^*(\boldsymbol{\nu}_r) = \begin{bmatrix} \tau_X \\ \tau_Y \\ \tau_N \end{bmatrix}, \tag{18}$$

at steady state one obtains

$$\begin{aligned} \tau_X &= -\left(m x_G - \left[\alpha Y_{\dot{r}} + (1-\alpha)Y_{\dot{r}}^-\right]\right) r^2 \\ &\quad - \left(m - Y_{\dot{v}}\right) r\, v_r - X_u u_r - X_{u|u|}\, u_r\, |u_r| \\ &= -\alpha\left(m x_G - Y_{\dot{r}}\right) r^2 - (1-\alpha)\left(m x_G - Y_{\dot{r}}^-\right) r^2 \\ &\quad - \left(m - Y_{\dot{v}}\right) r\, v_r - X_u u_r - X_{u|u|}\, u_r\, |u_r| \end{aligned} \tag{19}$$

$$\begin{aligned} \tau_Y &= \left(m - X_{\dot{u}}\right) u_r\, r - m y_G\, r^2 \\ &\quad - Y_v v_r - Y_{v|v|}\, v_r\, |v_r| \end{aligned} \tag{20}$$

$$\begin{aligned} \tau_N &= \left(m x_G - \left[\alpha Y_{\dot{r}} + (1-\alpha)Y_{\dot{r}}^-\right]\right) r\, u_r \\ &\quad + \left(m - Y_{\dot{v}}\right) v_r\, u_r - \left(m - X_{\dot{u}}\right) v_r\, u_r + m y_G\, r\, v_r \\ &\quad - \left[\alpha N_r + (1-\alpha)N_r^-\right] r \\ &\quad - \left[\alpha N_{r|r|} + (1-\alpha)N_{r|r|}^-\right] r\, |r| \\ &= \alpha\left(m x_G - Y_{\dot{r}}\right) r\, u_r + (1-\alpha)\left(m x_G - Y_{\dot{r}}^-\right) r\, u_r \\ &\quad + \left(m - Y_{\dot{v}}\right) v_r\, u_r - \left(m - X_{\dot{u}}\right) v_r\, u_r + m y_G\, r\, v_r \\ &\quad - \alpha N_r\, r - (1-\alpha)N_r^-\, r \\ &\quad - \alpha N_{r|r|}\, r\, |r| - (1-\alpha)N_{r|r|}^-\, r\, |r|. \end{aligned} \tag{21}$$

The above mentioned equations show how the components of $\boldsymbol{\tau}^*(\boldsymbol{\nu}_r)$ can be written as polynomial model, with the following coefficients:

$$\begin{aligned} \tau_X &= -\alpha c_{X,1} r^2 - (1-\alpha) c_{X,2} r^2 - c_{X,3} r v_r - c_{X,4} u_r \\ &\quad - c_{X,5} u_r |u_r| \end{aligned} \tag{22}$$

$$\begin{aligned} \tau_N &= \alpha c_{N,1}\, r\, u_r + (1-\alpha) c_{N,2}\, r\, u_r + c_{N,3}\, v_r\, u_r \\ &\quad + c_{N,4}\, r\, v_r - \alpha c_{N,5}\, r - (1-\alpha) c_{N,6}\, r \\ &\quad - \alpha c_{N,7}\, r\, |r| - (1-\alpha) c_{N,8}\, r\, |r|. \end{aligned} \tag{23}$$

As it will be shown in the following, the sway equation is not strictly necessary for a control oriented identification, and consequently is not parametrized.

Notice that according to the derived model, parameters $c_{X,1}$, $c_{X,2}$ and $c_{X,3}$ should be equal to $c_{N,1}$, $c_{N,2}$ and $c_{N,3}$ respectively. Nevertheless, the identification procedure has been implemented assuming such parameters to be possibly different. The reason for this is ultimately related to identifiability considerations: given that the parameters multiply different combination of state variables, depending on the maneuver, it may happen (by example) that $c_{X,1}$ is identifiable and $c_{N,1}$ is not. In a similar situation, it is best to delete the entire term relative to the non identifiable parameter $c_{N,1}$ rather than to keep it in the system of equations forcing the parameter to correspond to $c_{X,1}$. Indeed both solutions were tested: forcing $c_{X,1}$, $c_{X,2}$ and $c_{X,3}$ to correspond to $c_{N,1}$, $c_{N,2}$ and $c_{N,3}$ respectively, and keeping them distinct. In the latter case, one of the two parameters was systematically non identifiable and setting it to zero provided a better overall fit than obtained in the former case. As a result, in the following we only consider the case where the parameters $c_{X,1}$, $c_{X,2}$ and $c_{X,3}$ are distinct from $c_{N,1}$, $c_{N,2}$ and $c_{N,3}$.

4. Proposed inverse model

4.1. Inverse thruster force to RPM relationship

We are now interested in finding out what RPM speed should a single motor have to exert a desired force F^*. Let us focus on one thruster only, and let us suppose that $n > 0$. Then, (8) becomes

$$b_1 n^2 - b_2 n u_m - F^* = 0, \tag{24}$$

which yields two solutions

$$n = \frac{b_2 u_m \pm \sqrt{b_2^2 u_m^2 + 4 b_1 F^*}}{2 b_1}, \; b_2^2 u_m^2 + 4 b_1 F^* > 0 \tag{25}$$

that are valid if and only if $n > 0$. It is easy to see that if $F^* > 0$, then only one solution is positive. However, if $-b_2^2 u_m^2 < 4 b_1 F^* < 0$ then two positive solutions exist for n. Notice that these two solutions appear only if $b_2 > 0$ and $F^* < 0$. A dual result is obtained when one considers $n < 0$. Hence, for a given F^*, there might be up to three n solutions, of which only one has the same sign of F^*. As the term b_2 models losses due to the wake factor, and accordingly to conventional thruster speed control schemes (Sørensen et al., 1997; Smogeli et al., 2004), for the remainder of the paper we shall consider the single solution where n has the same sign as F^*, as implicitly done also in Skjetne et al. (2004). Finally notice that when applied to the port and starboard thrusters, Eq. (25) will be evaluated with the corresponding $u_{m,p}$ and $u_{m,s}$ according to Eqs. (9).

4.2. Inverse body wrench to thruster forces relationship

Let us now consider the inverse relationship between the body wrench and the thruster forces. At steady state it holds that

$$\boldsymbol{\tau}^*(\boldsymbol{\nu}_r) = \boldsymbol{B}(\boldsymbol{n}^*)\boldsymbol{f}(\boldsymbol{n}^*) = \boldsymbol{\tau}_c(\boldsymbol{n}^*), \tag{26}$$

which means that $\boldsymbol{\tau}^* \in \mathrm{Span}(\boldsymbol{B}) \in \mathbb{R}^2$. In lieu of the fact that $\boldsymbol{B}$ spans only a two dimensional subspace, and since we are interested in finding out the steady state thruster forces $\boldsymbol{f}(\boldsymbol{n}^*)$ we can consider the first and third equation only (since they are always linearly independent, while the sway one could be linearly dependent to the surge one depending on the actual coefficients k_p and k_s), obtaining

$$\begin{aligned} \bar{\boldsymbol{\tau}}^* &\triangleq \begin{bmatrix} \tau_X^* \\ \tau_N^* \end{bmatrix} = \bar{\boldsymbol{B}}(\boldsymbol{n}^*)\boldsymbol{f}(\boldsymbol{n}^*) \\ &\triangleq \begin{bmatrix} 1 & 1 \\ d + l k_p(n_p) & -d + l k_s(n_s) \end{bmatrix} \begin{bmatrix} F_p(n_p^*) \\ F_s(n_s^*) \end{bmatrix}, \end{aligned} \tag{27}$$

whose inverse allows to compute the steady state thruster forces corresponding to a steady state body wrench

$$\begin{aligned} F_p^* &= \frac{(d - k_s l)\,\tau_X^* + \tau_N^*}{2d + k_p l - k_s l}, \\ F_s^* &= \frac{(d + k_p l)\,\tau_X^* - \tau_N^*}{2d + k_p l - k_s l}. \end{aligned} \tag{28}$$

Due to the dependency of $\bar{\boldsymbol{B}}$ on the sign of the components of $\boldsymbol{n}^*$, there are actually four possible matrices $\bar{\boldsymbol{B}}$, each one corresponding to a particular couple of signs for n_p and n_s and therefore assignment of k^+ and k^- to k_p and k_s. In the direct model, this ambiguity is easily solved as the signs of n_p and n_s are known. When inverting the equation, the signs of n_p and n_s are instead unknown. Since the sign of F corresponds to the sign of n, to solve this ambiguity one has to assume the signs of n_p and n_s, instantiate k_p and k_s with the corresponding k^+ or k^- values, compute the resulting steady state thruster forces using (28), and verify that the signs of the forces correspond to the assumption made. These steps are repeated for the four possible combinations of signs, until a solution satisfying the assumption is found.

A numerical analysis has shown that the four matrices span subregions of $\mathbb{R}^2$ which sum up to the whole $\mathbb{R}^2$. An example of the "spans" is depicted in Fig. 2. Two matrices $\bar{\boldsymbol{B}}$ corresponding to different choices for k_p and k_s share, as possible valid output, only the half line corresponding to the *same* column (if any). The overlap happens when the column that corresponds to different signs is actually multiplying a zero force, therefore it is irrelevant. The aforementioned remarks are true under the conditions

$$\begin{cases} k^+ > -\frac{2d}{l} + k^- \\ k^- > -\frac{2d}{l} + k^+ \end{cases}. \tag{29}$$

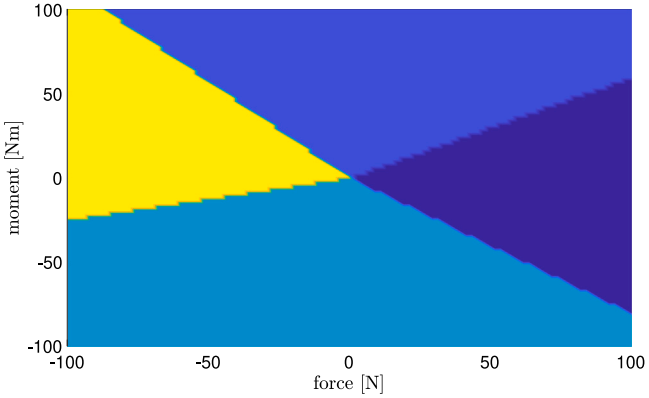

Fig. 2. Image subregions of the four possible $\bar{\boldsymbol{B}}$ matrices. Example taken from the experiments, where the identified values are $k^+ = 0.07$ and $k^- = 0.3$. Dark blue area: $k_p = k_s = k^+$, blue area: $k_p = k^+$, $k_s = k^-$, cyan area: $k_p = k^-$, $k_s = k^+$, yellow area: $k_p = k_s = k^-$). (For interpretation of the references to color in this figure legend, the reader is referred to the web version of this article.)

Algorithm 1 $[\hat{n}_p, \hat{n}_s] = \mathrm{InverseModel}(u_r, r, \boldsymbol{c})$

1: $u_{m,p}, u_{m,s} \leftarrow$ updated according to port/starboard (9)
2: $\tau_X \leftarrow$ updated using the first equation of (22)
3: $\tau_N \leftarrow$ updated using the second equation of (22)
4: $F_p^*, F_s^* \leftarrow$ updated according to port/starboard (28)
5: $\hat{n}_p \leftarrow$ unique solution of (25) of the same sign of F_p^*, using b_1 and b_2 as in (10)
6: $\hat{n}_s \leftarrow$ unique solution of (25) of the same sign of F_s^*, using b_1 and b_2 as in (10)
7: **return** $[\hat{n}_p, \hat{n}_s]$

Notice that $k^+ = -\frac{2d}{l} + k^-$ and $k^- = -\frac{2d}{l} + k^+$ actually represents the only two cases for which a matrix $\bar{\boldsymbol{B}}$ is singular. In our case, (29) defines a region of the plane k^+, k^- that contains the whole interval $k^+ \in [0, 0.93]$ and $k^- \in [0, 0.93]$, which contains and exceeds the expected ranges for these parameters. Given these practical considerations, from now on we will assume the existence and the uniqueness of the solution.

5. Identification procedure

The identification procedure used in this work is quite simple from an experimental point of view. It requires having the steady state correspondences between known constant thruster RPMs (n_p, n_s) and the resulting steady state relative surge and yaw rate velocities (u_r, r) resulting from GNSS and inertial measurements.

The procedure works as follows. From a given steady state velocity (u_r, r), the procedure exploits the hydrodynamic parameters to compute the wrench acting on the body (see (22)). Then, it allocates such a wrench to compute the two steady state thruster forces using (28) (and solving for the ambiguity on $\bar{\boldsymbol{B}}$). Finally, it inverts the thruster equation to find which RPM velocity is required to produce such a force, using (25) and the associated motor parameters (in four quadrants, see (10)). At the end of the procedure, two estimated motor velocities $(\hat{n}_p, \hat{n}_s)$ have been computed. Such a procedure, denominated InverseModel(), is reported in Algorithm 1. The vector $\boldsymbol{c}$ groups all the eight thruster parameters in (10), the hydrodynamics parameters in (22), and the two parameters k^+ and k^- to model the transverse thrust.

To find the best vector of parameters $\boldsymbol{c}$, a numerical nonlinear least squares method has been used to fit the outputs $(\hat{n}_p, \hat{n}_s)$ of the function InverseModel() to the experimental data of RPMs (n_p, n_s), knowing the corresponding u_r, r values. The nonlinear least squares algorithm employed is a trust-region-reflective algorithm, namely a subspace

(a) (b)

Fig. 3. (a) The ULISSE ASV without any additional payloads. The two aluminum profiles running along the length of both hulls can be used to install customized decks. (b) the above-deck WiMUST configuration with the acoustic sparker.

trust-region method. This is based on the interior-reflective Newton method described in Coleman and Li (1994, 1996). Each iteration involves the approximate solution of a large linear system using the method of preconditioned conjugate gradients.

6. Models experimental validation and comparison

To evaluate the proposed model an experimental data set has been collected using the ULISSE ASV, which is presented in the following subsection.

6.1. The ULISSE ASV

The ULISSE ASV, shown in Fig. 3, is a 3 m long and 1.8 m wide catamaran, constructed in fiberglass. It is the second generation of catamarans developed by ISME - University of Genova, following a first design in 2015 that was conceived for a private company (Simetti et al., 2016). The two hulls have identical geometry and are fixed together by two carbon fiber bars, that pass through the two hulls below the deck line, and are fixed on both the interior and exterior of the catamaran. In each hull, a compartment hosts the batteries (around 3.2 kWh energy each) and the control electronics including inertial sensors (compass, accelerometers and gyroscopes). A Global Navigation Satellite System (GNSS) antenna is placed on top of the roll bar.

Propulsion is guaranteed by two Torqeedo Cruise 2R electric propeller motors, with an electrical power of 2 kW and around 50% propulsive efficiency. The two motors are identical, and rotate clockwise for positive RPMs and anti-clockwise for negative RPMs. Therefore, it is expected that a transverse thrust is generated, pulling the stern to starboard when the vessel is moving forward. Hence, a negative yaw-rate is expected when the motors are set to the same positive RPMs.

Each motor takes as input a pulse width modulation value $h \in [-100\%, 100\%]$ through a RS485 bus. The same bus allows accessing the actual motor RPM, measured with Hall effect sensors. In all our experiments the command h was limited to $\pm 80\%$, and a linear relationship has been experimentally witnessed between the propeller RPM (revolutions per minute) n and the commanded percentage, i.e. $n = \lambda h$. However, the factor λ is asymmetric with respect to the sign of the command, that is:

$$n = \begin{cases} \lambda_+ h, & h \geq 0 \\ \lambda_- h, & h < 0 \end{cases} \tag{30}$$

with $\lambda_+ > 0$, $\lambda_- > 0$ and $\lambda_+ \neq \lambda_-$. Using the maximum propeller revolution rate, extracted from the motor datasheet and reported in Table 1, it follows that $\lambda_+ = 13$, while from bench experiments, λ_- has been evaluated to be roughly as the 70% of λ_+. Furthermore, as propellers' shape is optimized for forward advancement, the thrust produced by the propeller for a given RPM value while going in reverse is reduced compared to the same positive RPM.

Table 1
Main characteristics of the ULISSE ASV.

Parameter	Value
Length	3 m
Width	1.8 m
Mass	400 kg
Maximum payload	200 kg
Electric motor power (single motor)	2000 W
Propulsive power (single motor)	1120 W
Motor static thrust (single motor)	512 N
Maximum propeller revolution rate	1300 RPM
Available power for payloads	25 A @ 24 V
Wireless	5 GHz Ubiquiti

6.2. Experimental validation

To collect the experimental data set needed to validate experimentally the proposed model, several experiments have been executed setting the thruster percentage h of both ULISSE motors to constant values letting the ASV move on steady state trajectories (either circles or straight lines depending on the difference in port and starboard thruster percentages). On circular trajectories the ASV was always doing at least a full circle before being stopped: the surge and yaw velocities associated to the test were then computed by taking the average value of the GNSS surge and yaw measurements over the whole trajectory in order to filter out possible effects of wind and currents (apparently absent during the trials) on the acquired data. Notice that in view of the fact that environmental conditions were very calm and test were designed to average out the effects of currents and wind, the acquired (u, r) measurements are assumed to coincide with (u_r, r) measurements.

Once the data set was available, several fits have been executed. To evaluate the quality of each fit, let us indicate with $\hat{c}$ the model parameters identified using the procedure and the nonlinear least squares approach described in Section 5. Then, the modeling error in RPM space is

$$\tilde{\boldsymbol{n}}_k = \boldsymbol{n}_k - \hat{\boldsymbol{n}}_k \tag{31}$$

being $\boldsymbol{n}_k$ the kth experimental thruster RPM vector and $\hat{\boldsymbol{n}}_k$ the expected one computed through Algorithm 1 with $\boldsymbol{c} = \hat{\boldsymbol{c}}$. To compare each fit, we used the root mean square fitting error (RMSE) associated to (31), i.e.

$$\sqrt{\sum_{k=1}^{N} \frac{1}{N} \|\tilde{\boldsymbol{n}}_k\|^2} \ . \tag{32}$$

The identified coefficients $\hat{c}$ and the associated RMSE results are summarized in Table 2. Following standard practice in the reporting of uncertainties (Taylor, 1997), these have been rounded to one significant figure in Table 2. Notice that the results have been obtained identifying the different models on the *same* data set.

The confidence intervals reported Table 2 for the parameter estimates are computed based on the hypothesis that they follow an asymptotic normal distribution. In particular such intervals refer to a 95% confidence region and result from the implementation of an off-the-shelf approach for nonlinear regression as described in Bates and Watts (1988).

First, let us remark that b_1^{++} is not identifiable: indeed, given the very structure of Eqs. (24) and (8), being n the measurement, any scalar multiplying the measurement vector will not be identifiable. In view of the non identifiability of b_1^{++}, this was *a priori* fixed to a value $\hat{b}_1^{++}$ derived from the thruster datasheets. In particular, we have set $\hat{b}_1^{++} = 3.03 \times 10^{-4}$ corresponding to the maximum static thrust (512 N) at the maximum RPM (1300).

Second, analyzing the acquired data, as expected, we noticed that the sway value was small (less than 20 cm/s almost everywhere in the

Table 2
Results of the model parameters fitting on the same data set. The column "variable" states the quantity that the parameter multiplies, if any. Whenever a parameter could not be fitted, we put a "–" symbol in the table. Instead, a "N/A" symbol represents a parameter who is not present in the respective model. The total available parameters for a given model are reported in the row "Total parameters", while those that could be effectively identified are reported in the row "Identified parameters".

Variable	Param.	Param. Units	Baseline	M1	M2 (proposed)
r^2	$c_{X,1}$	$[N][s]^2$	–	–	–
u	$c_{X,4}$	$\frac{[N][s]}{[m]}$	–	–	–
$u\|u\|$	$c_{X,5}$	$\frac{[N][s]^2}{[m]^2}$	−17 ± 7	−58 ± 16	−62 ± 13
ru	$c_{N,1}$	$[N][s]^2$	(8 ± 4) 10	(4.7 ± 1.5) e2	(46 ± 9) 10
r	$c_{N,5}$	[N][m][s]	–	–	–
$r\|r\|$	$c_{N,7}$	$[N][m][s]^2$	(−1 ± 0.2) e3	(−3.9 ± 3) e2	–
r^2 $(\alpha = 0)$	$c_{X,2}$	$[N][s]^2$	N/A	–	–
ru $(\alpha = 0)$	$c_{N,2}$	$[N][s]^2$	N/A	(−2.4 ± 1.6) e2	–
r $(\alpha = 0)$	$c_{N,6}$	[N][m][s]	N/A	–	–
$r\|r\|$ $(\alpha = 0)$	$c_{N,8}$	$[N][m][s]^2$	N/A	(−1.2 ± 0.4) e3	(−1.3 ± 0.3) e3
$\|n\|n$	b_1^{++} (fixed)	$\frac{[N]}{[rpm]^2}$	3.03e−4	3.03 e–4	3.03 e–4
$\|n\|u_m$	b_2^{++}	$\frac{[N][s]}{[rpm][m]}$	(7.2 ± 1.3) e–2	–	–
$\|n\|n$	b_1^{+-}	$\frac{[N]}{[rpm]^2}$	(1.6 ± 0.4) e–4	N/A $(= b_1^{++})$	N/A $(= b_1^{++})$
$\|n\|u_m$	b_2^{+-}	$\frac{[N][s]}{[rpm][m]}$	–	N/A $(= b_2^{++})$	N/A $(= b_2^{++})$
$\|n\|n$	b_1^{-+}	$\frac{[N]}{[rpm]^2}$	(1.6 ± 0.6) e–4	N/A $(= b_1^{--})$	N/A $(= b_1^{--})$
$\|n\|u_m$	b_2^{-+}	$\frac{[N][s]}{[rpm][m]}$	–	N/A $(= b_2^{--})$	N/A $(= b_2^{--})$
$\|n\|n$	b_1^{--}	$\frac{[N]}{[rpm]^2}$	(1.4 ± 0.4) e–4	(1.5 ± 0.4) e–4	(1.4 ± 0.4) e–4
$\|n\|u_m$	b_2^{--}	$\frac{[N][s]}{[rpm][m]}$	(9 ± 4) e–2	(3.0 ± 2.1) e–2	–
	k^+	–	N/A	N/A	(7.3 ± 1.5) e-2
	k^-	–	N/A	N/A	(3.5 ± 0.7) e-1
	RMSE	rpm	70.9	62.2	53.9
	Total par.	–	14	14	16
	Identified par.	–	9	8	7

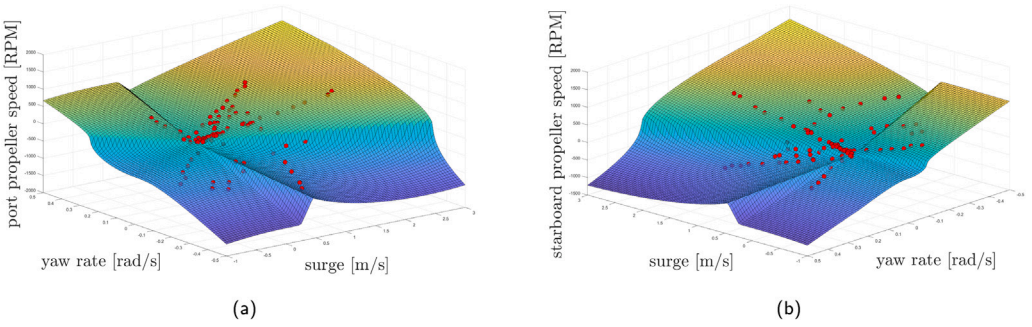

Fig. 4. Results of the proposed model (M2) fit in terms of thruster RPMs at steady state, where the red dots represent the experimental value of the thruster RPM: (a) port thruster, (b) starboard thruster. (For interpretation of the references to color in this figure legend, the reader is referred to the web version of this article.)

plane (u_r, r)), and characterized by quite some noise, probably due to the fact that sway has been computed from GNSS speed data through projection on the transversal axis of the robot using magnetometer data. Given these considerations, we assumed $v_r \approx 0$ and neglected the corresponding parameters $c_{X,3}, c_{N,3}, c_{N,4}$ in (22) for all the discussed models. Ex-post, this assumption appears to be very reasonable, as the proposed model fits indeed well.

For each model reported in the table, we started the fit with all the available parameters. If the fit result had parameters whose confidence interval included zero, we ran the fitting procedure again removing those parameters. Whenever a parameter could not be fitted, we put a "-" symbol in the table. Instead, a "N/A" symbol represents a parameter that is not present in the respective model.

The first model reported in the table is the baseline model, discussed in Section 2, which has the worst fitting performance. Out of 14 available parameters, 9 are identified leading to an RMSE of 70.9. The second model (M1) reported in the table models the drag at different operating points, as discussed in Section 3.1. With just 8 identified parameters, the model provides a better fit, with an RMSE of 62.2. It is interesting to note the higher coefficient of $r|r|$ when $\alpha = 0$ with respect to $\alpha = 1$, due to one of hulls moving backwards.

Finally, the table shows the result of the proposed model (M2), which also includes transverse thrust effects, as discussed in Section 3.2. In this case, despite an overall higher number of parameters available, actually only 7 results identifiable, leading to even better results in terms of RMSE (53.9), namely over 13% reduction of the RMSE of model M1 and 24% of the baseline model. With respect to the model M1, three parameters are not anymore identified (the coefficients multiplying $r|r|$, ru for $\alpha = 0$ and b_2^{--}). In particular, the model M2 does not identify both r and $r|r|$ angular drag coefficients for $\alpha = 1$. While from a first principles point of view at least one of the two parameters should not be zero, two remarks should be made. First, the rotations on the spot (i.e., the points placed in the vicinities of $u_r = 0$) belong to the case $\alpha = 0$, for which the relative parameter $r|r|$ is actually identified. The points of the (u_r, r) plane contributing to the identification of the angular drag parameters for $\alpha = 1$ are

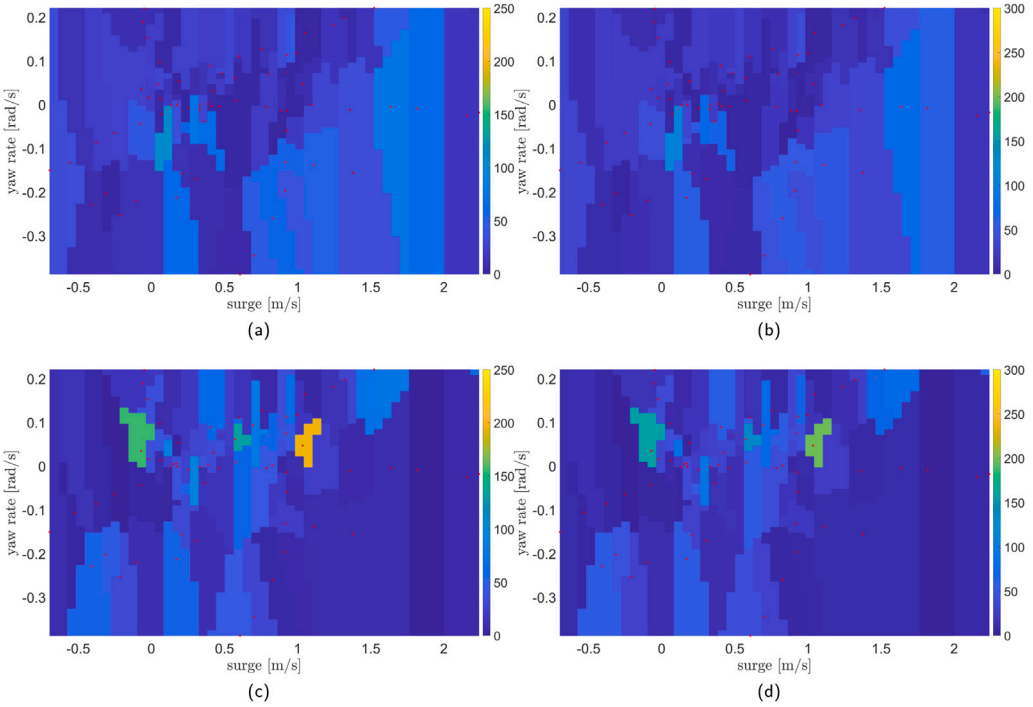

Fig. 5. Absolute RPM errors maps: the red dots indicate the points for which experimental data is available. The remainder of the plane is colored according to the closest data point (dark colors are better). (a) port thruster error for the baseline model (b) port thruster error for the proposed model (M2); (c) starboard thruster error for the baseline model (d) starboard thruster error for the proposed model (M2). (For interpretation of the references to color in this figure legend, the reader is referred to the web version of this article.)

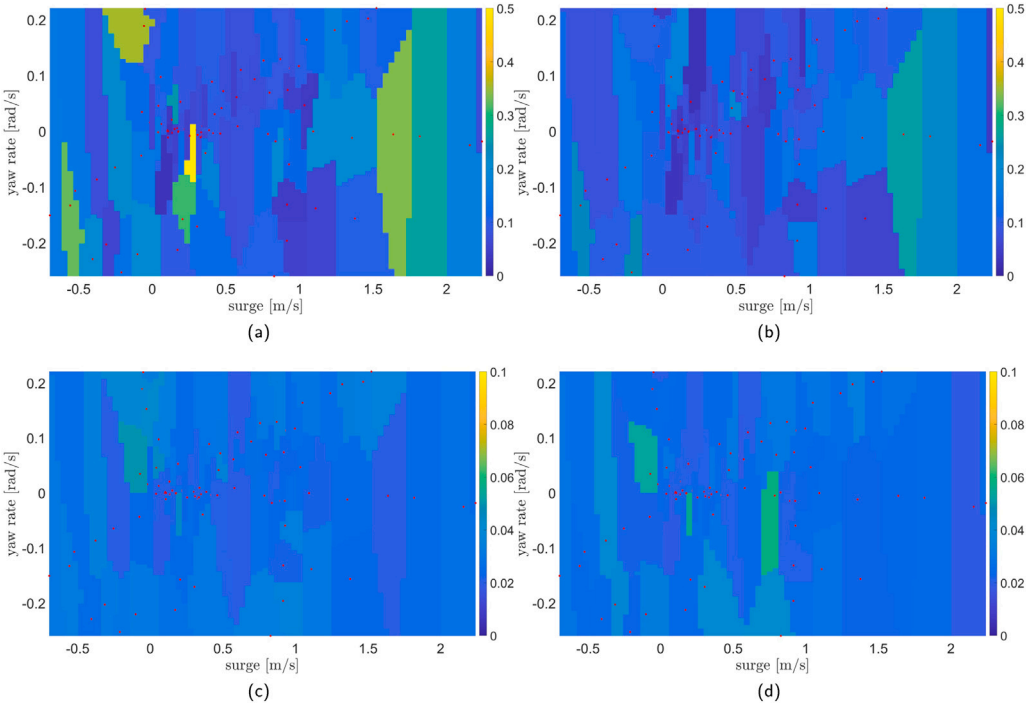

Fig. 6. Steady state error maps: the red dots indicate the points for which experimental data is available. The remainder of the plane is colored according to the closest data point (dark colors are better). (a) surge error for the baseline model (b) surge error for the proposed model (M2); (c) yaw rate error for the baseline model (d) yaw rate error for the proposed model (M2). (For interpretation of the references to color in this figure legend, the reader is referred to the web version of this article.)

all located at $u_r > 0$, where $r|r|$ might be similar to ru. Second, the addition of the parameters k^+, k^- modifies the overall moment and contributes to making those parameters non identifiable. It is however remarkable that the proposed model obtains *better* results with *less* parameters, which suggests that the newly introduced parameters are more important and predominant from a modeling point of view.

Notice that for both M1 and the proposed model M2 we have differentiated only two quadrants (i.e., a set of b_1 and b_2 parameters for $n > 0$ and one for $n < 0$, without differentiating with respect to the

sign of u_m). Fitting tests with free parameters for all four quadrants were conducted, but resulted in fits that were only slightly better. The new motor parameters were $b_x^{+-} \approx b_x^{++}$ and $b_x^{-+} \approx b_x^{--}$, hence very similar to the assumption made in M1 and M2. Furthermore, the addition of those free parameters increased the uncertainty bounds on all the others. Therefore, such models were omitted from Table 2 for the sake of brevity. The final fit of the proposed model for both port and starboard thrusters is reported in Fig. 4.

To further compare the fits, Fig. 5 shows the absolute RPM error maps for the baseline and the proposed model (M2), for both port and starboard thrusters. The plots highlight the overall better fit of the proposed model, for both thrusters.

A final comparison has been done using the hydrodynamic models to predict the ASV velocity, as one would do in a navigation filter. To this aim, the same inertia matrix has been used for both models, and only the steady state values $\hat{u}_r, \hat{r}$ were logged. Then, for each trial, the integral of the absolute error was computed separately for the surge and yaw rate values. The results of the errors are plotted in Fig. 6. The figure shows an overall better reproduction of the steady state velocities by the proposed model, especially at low speed.

7. Conclusions

This paper has investigated the modeling and identification of twin thruster ASVs. The manuscript shows that the typical models found in the literature do not fully capture and explain certain asymmetries and nonlinear behaviors of this type of vessels. The proposed model differentiates the hydrodynamic derivatives for the angular drag for two different operating points, namely when the ICR lies between the hulls (tight turns) or it is fully outside (straight course or large radius curves). Another important effect that has been modeled is the fact that even fixed-pitch propellers give rise to a transverse thrust, due to many effects as for example the paddle wheel effect, or pressure differential due to propellers generating reverse thrust. The paddle-wheel effect is especially relevant for vessels with two non-counterotating thrusters, such as most of the robot catamarans, as they do not compensate each other. An experimental data set has been acquired and used to show the improvements of the proposed model with respect to the baseline one.

Future works will be aimed at exploiting this improved model for control purposes, comparing several approaches for the dynamic control of the ASV. Furthermore, we aim to acquire a more precise inertial navigation system including a Doppler Velocity Logger and a fiber optic gyro, to increase the accuracy and precision of the inertial data, allowing for sway parameters identification too.

CRediT authorship contribution statement

Enrico Simetti: Conceptualization, Methodology, Software, Data curation, Writing – original draft. **Giovanni Indiveri:** Conceptualization, Methodology, Writing – review & editing.

Declaration of competing interest

The authors declare that they have no known competing financial interests or personal relationships that could have appeared to influence the work reported in this paper.

Acknowledgments

The authors would like to thank all the SEALab members, the joint applied research laboratory between the Naval Experimentation and Support Centre (CSSN) of the Italian Navy and ISME, who helped the research team during the ULISSE development. We would also like to thank our colleague Prof. Michele Viviani for the fruitful discussions on propellers and vessels hydrodynamics.

References

Alves, J., Oliveira, P., Oliveira, R., Pascoal, A., Rufino, M., Sebastiao, L., Silvestre, C., 2006. Vehicle and mission control of the DELFIM autonomous surface craft. In: 2006 14th Mediterranean Conference on Control and Automation. IEEE, Ancona, Italy, pp. 1–6.

Bachmayer, R., Whitcomb, L.L., Grosenbaugh, M.A., 2000. An accurate four-quadrant nonlinear dynamical model for marine thrusters: Theory and experimental validation. IEEE J. Ocean. Eng. 25 (1), 146–159. http://dx.doi.org/10.1109/48.820747.

Bates, D.M., Watts, D.G., 1988. Nonlinear Regression Analysis and its Applications. John Wiley & Sons, Inc..

Caccia, M., Bibuli, M., Bono, R., Bruzzone, G., 2008. Basic navigation, guidance and control of an unmanned surface vehicle. Auton. Robots 25 (4), 349–365.

Caccia, M., Bruzzone, G., Bono, R., 2006. Modelling and identification of the Charlie2005 ASC. In: 2006 14th Mediterranean Conference on Control and Automation. IEEE, Ancona, Italy, pp. 1–6. http://dx.doi.org/10.1109/MED.2006.328785.

Carlton, J., 2018. Marine Propellers and Propulsion. Butterworth-Heinemann.

Coleman, T.F., Li, Y., 1994. On the convergence of interior-reflective Newton methods for nonlinear minimization subject to bounds. Math. Program. 67 (1), 189–224.

Coleman, T.F., Li, Y., 1996. An interior trust region approach for nonlinear minimization subject to bounds. SIAM J. Optim. 6 (2), 418–445.

Curcio, J., Leonard, J., Patrikalakis, A., 2005. SCOUT - a low cost autonomous surface platform for research in cooperative autonomy. In: Proceedings of OCEANS 2005 MTS/IEEE. Washington, DC, USA, pp. 725–729. http://dx.doi.org/10.1109/OCEANS.2005.1639838.

Du, J., Hu, X., Krstić, M., Sun, Y., 2018. Dynamic positioning of ships with unknown parameters and disturbances. Control Eng. Pract. 76, 22–30.

Dunbabin, M., Grinham, A., Udy, J., 2009. An autonomous surface vehicle for water quality monitoring. In: Australasian Conference on Robotics and Automation (ACRA). Sydney, Australia, pp. 1–6.

Ebken, J., Bruch, M., Lum, J., 2005. Applying unmanned ground vehicle technologies to unmanned surface vehicles. In: SPIE Unmanned Ground Vehicle Technology VII. Orlando, FL, USA, pp. 585–596. http://dx.doi.org/10.1117/12.605254.

Elkins, L., Sellers, D., Monach, W.R., 2010. The autonomous maritime navigation (AMN) project: Field tests, autonomous and cooperative behaviors, data fusion, sensors, and vehicles. J. Field Robotics 27 (6), 790–818. http://dx.doi.org/10.1002/rob.20367.

Eriksen, B.-O.H., Breivik, M., 2017. Modeling, identification and control of high-speed ASVs: Theory and experiments. In: Sensing and Control for Autonomous Vehicles, Vol. 47. Springer, pp. 407–431.

Ferreira, H., Almeida, C., Martins, A., Almeida, J., Dias, N., Dias, A., Silva, E., 2009. Autonomous bathymetry for risk assessment with ROAZ robotic surface vehicle. In: Oceans 2009-Europe. IEEE, Bremen, Germany, pp. 1–6. http://dx.doi.org/10.1109/oceanse.2009.5278235.

Fossen, T.I., 1994. Guidance and Control of Ocean Vehicles. John Wiley & Sons Inc.

Fossen, T.I., 2011. Handbook of Marine Craft Hydrodynamics and Motion Control. John Wiley & Sons.

Fossen, T.I., 2012. How to incorporate wind, waves and ocean currents in the marine craft equations of motion. In: 9th IFAC Conference on Manoeuvring and Control of Marine Craft, Vol. 45. pp. 126–131. http://dx.doi.org/10.3182/20120919-3-IT-2046.00022.

Guerreiro, B.J., Silvestre, C., Cunha, R., Pascoal, A., 2014. Trajectory tracking nonlinear model predictive control for autonomous surface craft. IEEE Trans. Control Syst. Technol. 22 (6), 2160–2175. http://dx.doi.org/10.1109/TCST.2014.2303805.

Haseltalab, A., Negenborn, R.R., 2019. Adaptive control for autonomous ships with uncertain model and unknown propeller dynamics. Control Eng. Pract. 91, 104116.

Häusler, A.J., Saccon, A., Hauser, J., Pascoal, A.M., Aguiar, A.P., 2015. A novel four-quadrant propeller model. In: Fourth International Symposium on Marine Propulsors (SMP 15), Austin, Texas, USA, pp. 498–506.

Liu, Z., Zhang, Y., Yu, X., Yuan, C., 2016. Unmanned surface vehicles: An overview of developments and challenges. Annu. Rev. Control 41, 71–93. http://dx.doi.org/10.1016/j.arcontrol.2016.04.018.

Majohr, J., Buch, T., 2006. Modelling, simulation and control of an autonomous surface marine vehicle for surveying applications measuring dolphin MESSIN. In: Roberts, G., Sutton, R. (Eds.), Advances in Unmanned Marine Vehicles. In: IEE Control Series, Institution of Engineering and Technology, pp. 329–351, (Chapter 16).

Manley, J., 1997. Development of the autonomous surface craft ACES. In: Oceans '97. MTS/IEEE Conference Proceedings, Vol. 2, Halifax, Nova Scotia, Canada, pp. 827–832.

Marquardt, J.G., Alvarez, J., von Ellenrieder, K.D., 2013. Characterization and system identification of an unmanned amphibious tracked vehicle. IEEE J. Ocean. Eng. 39 (4), 641–661.

Naeem, W., Xu, T., Sutton, R., Tiano, A., 2008. The design of a navigation, guidance, and control system for an unmanned surface vehicle for environmental monitoring. Proc. Inst. Mech. Eng. M: J. Eng. Marit. Environ. 222 (2), 67–79.

Peeters, G., Boonen, R., Vanierschot, M., DeFilippo, M., Robinette, P., Slaets, P., 2018. Asymmetric steering hydrodynamics identification of a differential drive unmanned surface vessel. IFAC-PapersOnLine 51 (29), 207–212.

Peng, Z., Wang, J., Wang, D., Han, Q.-L., 2020. An overview of recent advances in coordinated control of multiple autonomous surface vehicles. IEEE Trans. Ind. Inf..

Pivano, L., Johansen, T.A., Smogeli, Ø.N., 2009. A four-quadrant thrust estimation scheme for marine propellers: Theory and experiments. IEEE Trans. Control Syst. Technol. 17 (1), 215–226.

Simetti, E., Indiveri, G., Pascoal, A.M., 2021. Wimust: A cooperative marine robotic system for autonomous geotechnical surveys. J. Field Robotics 38 (2), 268–288. http://dx.doi.org/10.1002/rob.21986.

Simetti, E., Torelli, S., Sperindé, A., 2016. Development of modular USVs for coastal zone monitoring. Sea Technol. 57 (05), 41–44.

Skjetne, R., Smogeli, Ø.N., Fossen, T.I., 2004. A nonlinear ship manoeuvering model: Identification and adaptive control with experiments for a model ship. Model. Identif. Control 25 (1), 3.

Smogeli, Ø.N., Sørensen, A.J., Fossen, T.I., 2004. Design of a hybrid power/torque thruster controller with loss estimation. IFAC Proc. Vol. 37 (10), 409–414.

Society of Naval Architects and Marine Engineers, 1950. Nomenclature for Treating the Motion of a Submerged Body Through a Fluid: Report of the American Towing Tank Conference. In: Technical and research bulletin, Society of Naval Architects and Marine Engineers.

Sonnenburg, C.R., Woolsey, C.A., 2013. Modeling, identification, and control of an unmanned surface vehicle. J. Field Robotics 30 (3), 371–398.

Sørensen, A.J., Ådnanes, A.K., Fossen, T.I., Strand, J.-P., 1997. A new method of thruster control in positioning of ships based on power control. IFAC Proc. Vol. 30 (22), 199–206.

Taylor, J.R., 1997. An Introduction to Error Analysis. University Science Books.

Vaneck, T., Manley, J., Rodriguez, C., Schmidt, M., 1996. Automated bathymetry using an autonomous surface craft. Navigation 43 (4), 407–418.

Whitcomb, L.L., Yoerger, D.R., 1999. Preliminary experiments in model-based thruster control for underwater vehicle positioning. IEEE J. Ocean. Eng. 24 (4), 495–506. http://dx.doi.org/10.1109/48.809273.

Wirtensohn, S., Reuter, J., Blaich, M., Schuster, M., Hamburger, O., 2013. Modelling and identification of a twin hull-based autonomous surface craft. In: 18th International Conference on Methods and Models in Automation and Robotics (MMAR). IEEE, pp. 121–126.

Woo, J., Park, J., Yu, C., Kim, N., 2018. Dynamic model identification of unmanned surface vehicles using deep learning network. Appl. Ocean Res. 78, 123–133.

Zereik, E., Bibuli, M., Mišković, N., Ridao, P., Pascoal, A., 2018. Challenges and future trends in marine robotics. Annu. Rev. Control 46, 350–368.